Perovskite CsPbI 2 Br Thin Films Prepared under Nitrogen Flow and Black Phase Stabilization in the Presence of a Two-Dimensional Inorganic Halide Material and Indium

Edouard Breniaux, Pascal Dufour, Karthick Sekar, Ceren Yildirim, Johann Bouclé, Sylvain Vedraine, Nicolas Ratel-Ramond, Christophe Tenailleau

EurJIC
European Journal of Inorganic Chemistry

Research Article
doi.org/10.1002/ejic.202200490

Chemistry Europe
European Chemical Societies Publishing

www.eurjic.org

Perovskite $CsPbI_2Br$ Thin Films Prepared under Nitrogen Flow and Black Phase Stabilization in the Presence of a Two-Dimensional Inorganic Halide Material and Indium

Edouard Breniaux,[a] Pascal Dufour,[a] Sekar Karthick,[b] Ceren Yildirim,[b] Johann Bouclé,[b] Sylvain Vedraine,[b] Nicolas Ratel-Ramond,[c] and Christophe Tenailleau*[a]

In this work, a simple thin films manufacturing process of all-inorganic halide perovskites has been developed under ambient conditions. A flow of nitrogen placed above the freshly deposited film by spin-coating, during the brief heat treatment stage, provides a suitable microstructure for photovoltaic applications. The main parameters of this process have been tested in order to obtain the most suitable perovskite layer for solar cells. Films of 3D $CsPbI_2Br$, mixtures of [3D + 2D] phases where $Cs_2PbCl_2I_2$ is the 2D material, and in the presence of indium in order to substitute lead in the main phase, were optimized and their structures analyzed by means of scanning electron microscopy and X-ray diffraction. Films are more compact and the structure tends to be more symmetrical upon doping, which preserve the black phase for a longer time. Each type of film was integrated into a fully functional solar cell. The addition of the 2D material to the main 3D phase affect the photovoltaic performances of the manufactured devices under our conditions but the photoactive black phase is clearly stabilized. A preferred orientation was observed in the presence of the 2D material and under nitrogen flow. Texture analysis evidenced for a fiber-like structure and the presence of indium tends to improve the black phase stability.

Introduction

Inorganic halide perovskites are very interesting structurally but also with great potential for various energetic applications including LEDs, ionizing radiation detectors and photovoltaics.[1–3] They are easy to prepare in different forms (crystals, powders, thin layers), usually crystallize near room temperature and exhibit a variety of structures. Thin films of inorganic halide perovskites have been recently under a large number of studies in order to prepare solar cells and optimize their efficiencies.[4–7] Dielectric screening effects can be used to tune their stability and efficiency.[8] Still, they suffer from instability and the black active phase changes quickly into a yellow non-perovskite structure. The black phase of $CsPbI_2Br$ is more stable than for $CsPbI_3$ and the former material, once integrated into a photovoltaic device, still exhibits an interesting solar conversion efficiency, above 17%.[9] In a recent study, we have shown that $CsPbI_2Br$ (and $CsPbI_3$) spontaneously crystallise with the gamma orthorhombic structure at room temperature and that mixing the perovskite (namely the 3D phase due to a three-dimensional interconnectivity of corner-shared octahedral environment surrounding each Pb^{2+} cation) with a two-dimensional or 2D material, namely $Cs_2PbCl_2I_2$, can improve the black phase stability.[10] This 2D material, discovered in 2018, possesses a Ruddlesden-Popper type structure, similarly to K_2NiF_4, with single layers of octahedra shifted from successive layers along the *c* axis and separated by double layers of large Cs^+ cations. It has been the subject of many different studies over the past years in order to substitute lead and understand their optoelectronic properties.[11–13]

The use of an argon or nitrogen atmosphere in a glove box is very often described in the literature to be a requirement to obtain stable thin films of halide perovskites, but it remains a strong limiting step for industrial upscaling. The use of nitrogen flow blown onto the substrate during crystallization stage is a process that is barely described, as heat treatment steps are often carried out in a glove box. However, some studies have shown the beneficial contribution of an air flow in order to control the heat treatment step of films containing perovskites.[14,15] Combining a hot-air assisted technique in ambient condition for the fabrication of quality $CsPbI_2Br$ thin films with the incorporation of Eu or In cations showed black to yellow phase transformation inhibition by releasing spontaneous strains in the lattice and passivation of traps.[16] In this work, DFT calculations showed a direct band gap and low cost hole transporting layers can lead to high efficiencies (close to 16%). A small amount of In^{3+} ions (1.5 mol.%) can improve the energy band alignment, reduce the exciton binding energy and hybrid perovskite-based solar cells can be stabilized over 3000 hours with 85% of the original (over 22%) efficiency.[17]

[a] E. Breniaux, P. Dufour, Dr. C. Tenailleau
CIRIMAT, Université de Toulouse, CNRS,
Université Toulouse 3 – Paul Sabatier,
118 Route de Narbonne, 31062 Toulouse cedex 9 – France
E-mail: christophe.tenailleau@univ-tlse3.fr
[b] S. Karthick, C. Yildirim, J. Bouclé, S. Vedraine
Université de Limoges, XLIM, CNRS, UMR 7252,
87000 Limoges, France
[c] N. Ratel-Ramond
CEMES-CNRS,
29 rue Jeanne Marvig, 31055 Toulouse, France

Research Article
doi.org/10.1002/ejic.202200490

A few recent studies have been undertaken under neutral gas such as argon or nitrogen and showed smooth films of packed grains after annealing.[18,19] This step is crucial because two phenomena take place in parallel: the evaporation of the solvent solubilizing perovskite precursors, and the crystallization of the perovskite, which thus passes from a solubilized state to a solid state when the solvent evaporates. Therefore, controlling precisely this step is very important for reproducibility reasons, but also for its effects on thin films microstructure and crystallinity.[20,21]

Here, we report an improved film compactness in a simple process of nitrogen flow and the stabilization of the $CsPbI_2Br$ black form in the presence of the 2D material and show the benefit of an indium substitution over the film stability. We also prepared complete stacks of layers including our perovskite-based mixtures in order to test solar cell efficiencies.

Results and discussion

Thin films of inorganic halide perovskites prepared in nitrogen flow

While three-dimensional halide perovskites are very common, two-dimensional inorganic halide perovskites are unusual and hardly found as pure single layers. We prepared thin films of $Cs_2PbCl_2I_2$ by spin-coating in ambient conditions a solution containing a mixture of the appropriate amount of salt precursors either in pure DMSO or DMF. A well-crystallized 2D material is evidenced by XRD analysis after hot-casting the film in air at 100 °C for 15 minutes. This process is a very simple synthetic route to prepare crystalline 2D materials-based thin layers. We decided to co-precipitate this 2D phase with the 3D $CsPbI_2Br$ phase in order to stabilize the latter and observe the effect of the 2D material over the film microstructure and device performances. In parallel, some authors have very recently showed that the same 2D material can act as a passivation layer and preserve a hybrid halide perovskite from air and humidity exposure, which is harmful for its properties, in particular for solar cells.[22]

During our previous detailed structural study performed on inorganic halide perovskites we showed that it was possible to stabilise the black form of the 3D main structure longer than usual thanks to presence of $Cs_2PbCl_2I_2$.[10] But the poor quality of the film obtained after in-situ XRD measurements could not be used for any type of electrical measurements. A flash thermal treatment just after spin-coating in air allowed us to form a more compact film. Thus, if we compare a thin film of $CsPbI_2Br$ phase flash-annealed at 320 °C with a [3D + 2D] mixture prepared in the same conditions, we can evidence that the black form of the perovskite phase is preserved one day longer in air once cooled down to room temperature. Figure 1 shows the XRD patterns of both materials deposited on ITO just after flash-sintering and 24 hours later, where the (hkl) planes corresponding only to the orthorhombic form of the black phase (known as the gamma phase) can still be evidenced after

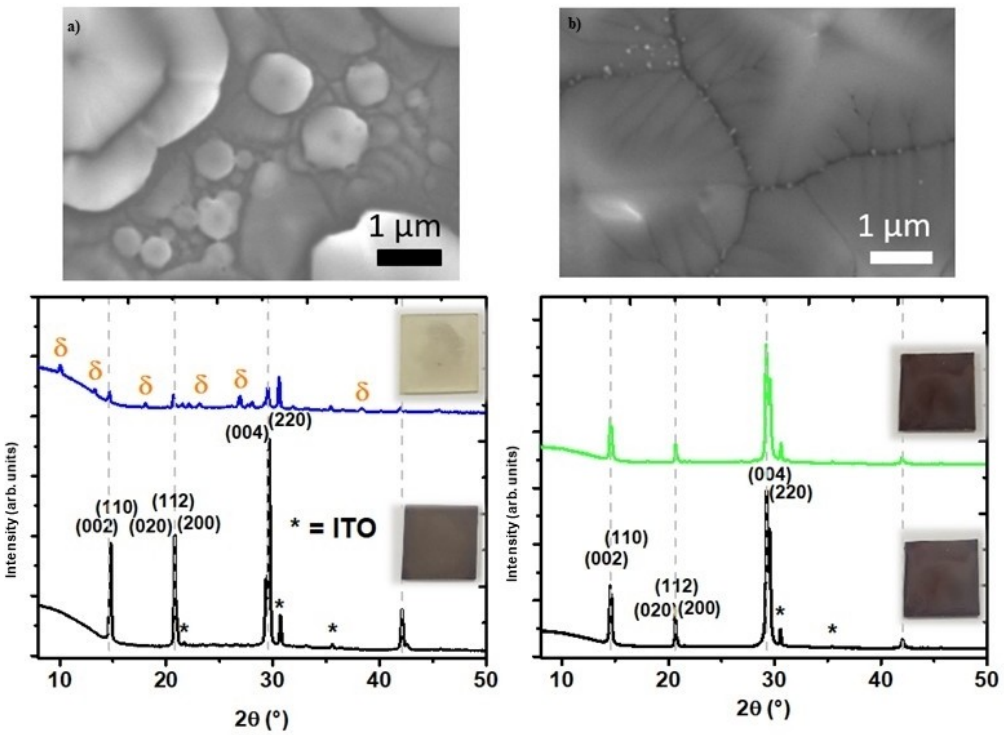

Figure 1. SEM images after 24 hours in air and XRD patterns of a) $CsPbI_2Br$ and b) [$CsPbI_2Br$ + 2D] mixture thin films, both spin-coated on ITO substrates and flash-sintered in air for 5 s at 320 °C. XRD shows a complete change of the black orthorhombic phase into the yellow delta phase within a day when the 2D material is not added. Insets are photos of the films.

Research Article
doi.org/10.1002/ejic.202200490

a day for the mixture. As evidenced by SEM images, the film microstructure is more homogenous and compact with the 2D material, with larger grains and small grain boundaries, justifying for the gain of stability in this case, but still required some improvements.

In order to obtain more compact films with no pinhole and avoid water penetration that degrades the black phase, we applied a nitrogen flow (nitrogen purity 4.5) positioned a few centimeters above the center of the hot plate used for hot-casting (Figure 2). After optimization, 1 mL of the solution was deposited on the substrate and spin-coated at a rate of 3000 rpm for 30 s in air. Then, the substrate was quickly introduced on the heating plate and under the nitrogen flow for 10 minutes.

If we compare SEM images of $CsPbI_2Br$ films deposited on FTO substrates and heated briefly at 200 °C, we can clearly see two different types of microstructures for heat treatments in air or under the nitrogen flow (Figure 3). For the first sample in air, an inhomogeneous film composed of large isolated grains is observed. However, for the second sample in N_2 flow a significantly more compact and homogeneous microstructure is obtained, composed of grains of sizes smaller than one micrometer due to fast solvent evaporation, saturation phase and crystallization. Film photographs also show homogeneity improvement of the surface as well as a reduction in edge effects, especially at the corners of the substrate. In fact, during the treatment of deposits in air, round shapes are often observed at the corners of the substrate, due to the agglomeration and a surface tension effect retaining an excess of solvent, which is incorrectly ejected during spin-coating. The nitrogen flow minimizes this effect by allowing homogeneous evaporation of the solvent over the entire surface of the substrate. XRD analysis shows the (hkl) lines of the orthorhombic black phase of the inorganic halide perovskite in both cases but for the air-treated sample extra-peaks corresponding to the yellow phase are already seen. For nitrogen flow-treated sample only the lines of the black form are identified with strong preferred orientations along the (hh0) and (00l) planes.

Different pressure flows and distances from the sample to the tip of the nozzle were tested and a maximum flow of 2 bars (0.9 L/s) generates pinholes in the films. By reducing the flow to 1 bar, the size of the pinholes appears to be smaller, although many holes are still seen on the film. By reducing the distance from 5 to 0.5 cm, the resulting film appears completely covering and the pinholes have disappeared, at this observation scale. On the other side, the distance of 0.1 cm reveals large clear and inhomogeneous domains in the deposit. The flow conditions at 1 bar with the end of the blower nozzle placed 0.5 cm from the heating plate therefore seem optimum to obtain the most homogeneous and covering deposit possible of perovskite. But

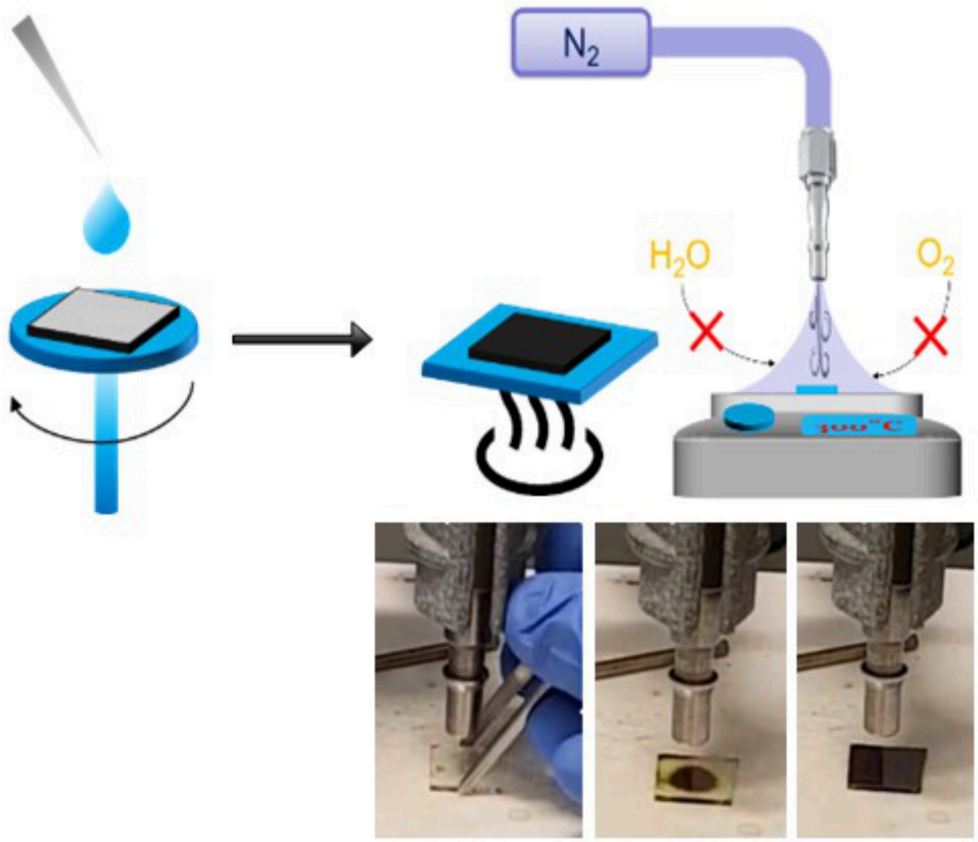

Figure 2. Experimental setup used for preparing our thin films. First, salt precursors and DMSO are deposited over the substrate and spin-coated. Second, the substrate covered by the film is directly put on the hot plate already set at a given temperature. Photos show that a black phase is formed by growing from the centre of the substrate to the edges.

Research Article
doi.org/10.1002/ejic.202200490

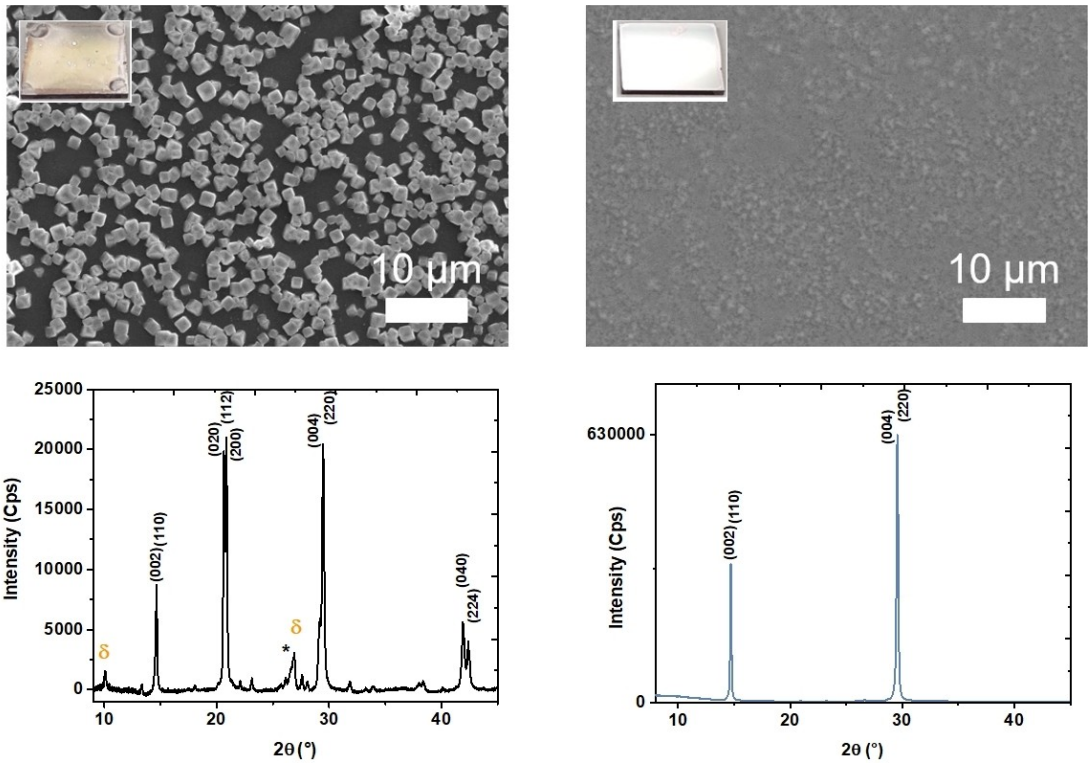

Figure 3. SEM images and photos of thin films of $CsPbI_2Br$ spin-coated on FTO substrates at 200 °C for 10 s in a) air and b) nitrogen flow, and corresponding XRD patterns (with the orthorhombic peak indexes used).

the process is strongly influenced by parameters related to the thickness of the limiting layer d.[21] By reducing the distance between the nitrogen source and the substrate, it is possible to minimize the value of d and make the film more homogeneous.

In order to improve the microstructure of the deposits, various heat treatment temperatures were also tested. In the literature, the values used for this step can vary from single to double. In our work, we will favor the use of several steps with a gradual rise in temperature in order to obtain the most interesting microstructure for a photovoltaic device, as reported in a previous work.[23] A low temperature (~50 °C) is preferred for this purpose for the first heat treatment step (T1). Then, each film (~300 nm in thickness) was annealed at a temperature T2 of 140 °C for 5 min followed by a third treatment at a temperature T3 of 300 °C for 10 min. The substrate appears then homogeneous and no pinholes are observed. We found that a gradual heat treatment in three stages gives the film of the best quality.

Influence of the indium addition in [3D + 2D] thin films

The replacement of lead by another element of the periodic table is a widely used technique for obvious reasons of toxicity. It also helps to stabilize the photoactive phase of perovskites. A significant number of chemical elements have already been integrated into the $CsPbI_2Br$ structure, with interesting effects such as increasing grain size, improving photovoltaic performance, or reducing defects.[16,17,24–28] Indium-doped $CsPbI_3$ films for inorganic perovskite solar cells with efficiency exceeding 17% were prepared in 2020.[29] Lead substitution by indium was also realized in Br-rich $CsPbIBr_2$ and the results have shown a marked improvement in device performance, notably by reducing crystal defects as well as improving absorption properties.[25] Enhanced stability was achieved in I-rich $CsPbI_2Br$ perovskite by means of In^{3+} and Cl^- co-doping.[28] This gives rise to a significant improvement in the overall spatial symmetry that would explain the long term stability. Indium was also selected because of its similar chemical properties to lead and tin, the three elements being classified in the family of poor metals. Indium has an adjustable degree of oxidation (+1 or +3) and a radius size (80 pm for In^{3+} against 120 pm for Pb^{2+}) potentially allowing it to integrate in substitution on the site of lead, despite a different valence state. Indium also has the ability to form a +2 oxidation state in the presence of halogens, by establishing In–In metal bonds.[30] This phenomenon could allow indium to have a different effect when integrated into perovskites, compared to bismuth for instance, which has a more rigid valence state that drives to the formation of microstresses and defects which reduce the grain size.[13,31]

In our previous work, we have shown that the perovskite crystallization process was slowed down in the presence of the 2D phase.[10] This crystallization process seems even further slowed down in the presence of indium. On the SEM images of Figure 4, it seems that the grains discernible at this resolution for the 3D phase are reduced in size for the [3D + 2D] mixture.

Research Article
doi.org/10.1002/ejic.202200490

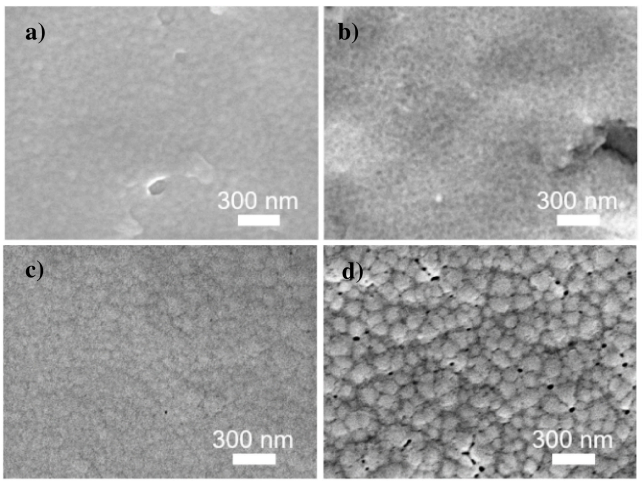

Figure 4. SEM images of perovskite layers prepared by spin-coating on FTO/SnO_2 substrates after three steps (50 °C for 2 min, then 140 °C for 5 min and 300 °C for 10 min) under nitrogen flow with a) 3D $CsPbI_2Br$, b) [3D + 2D] mixture, c) [3D + 2D + 5 mol.% In] mixture, and d) [3D + 2D + 10 mol.% In] mixture.

The composite created by the addition of 2D phase therefore promotes the formation of small grains that stabilize the black phase, as already noticed in a recent work.[32] However, as discussed previously, the increase in grain size is linked to improved photovoltaic efficiencies and reduced ion migration, as highlighted in a large number of articles in the literature.[33–35] The numerous grain boundaries would act as non-radiative recombination sites, thus limiting the voltage of the solar cells, when the grains size decreases. However, a study based on DFT calculations showed that structural relaxations at the grain boundaries lead to an improvement in the stability of the black phase of $CsPbI_3$, thereby generating deep trap levels which cause faster carrier recombination.[36] They have also shown that these grain boundaries can be passivated by adding halogenated elements or by doping. This passivation partially removes the trap levels that form at grain boundaries and can be achieved by introducing bromine to the iodine site, resulting in the formation of shallow trap levels. Intrinsic doping can also be achieved by growing the films under sub-stoichiometric conditions of iodine. This condition allows to increase the formation energy and thus prevent the formation of interstitial iodine in grains, and reduce the concentration of grain boundary defects. Subsequently, the additions of 5% and 10% indium were made in the [3D + 2D] mixture, ideally as a substitution on the lead site calculated for the $CsPbI_2Br$ phase (by introducing the appropriate amount of $InBr_3$ in the raw solution). The different microstructures obtained are also depicted in Figure 4. Composites with 5% then 10% indium show a gradual increase in grain size. These grains are interconnected and form a compact deposit, although the presence of pinholes was observed for the sample substituted at 10% indium. By reducing the rate of crystallization through its interaction with the solvent, indium thus makes it possible to modify the crystallization kinetics and the final microstructure of the film. The slowing down of the formation of perovskite allows the 2D phase to position itself at grain boundaries formed by the 3D phase, thereby creating larger crystal domains.

Figure 5 shows an ageing study over one week of thin films made with nitrogen blowing process with an increasing amount of indium. The 3D phase thin film is transformed into the yellow phase after 24 hours in air, while the [3D + 2D] mixture film remains stable for one more day. Adding 2.5% and 5% indium (calculated for lead substitution) increases the stability of the dark phase of the [3D + 2D] mixture for up to 4 days. The optimum indium addition rate determined by this method is 10% where the sample retains the black phase for 5 days, while an addition of 15% again reduces the stability of the black phase. The precursor of indium ($InBr_3$) being hygroscopic, it is therefore possible that beyond a certain level the indium favors the destabilization of the black phase by moisture absorption, when it is not integrated in the crystalline structure.

The influence of the intended substitution of lead by indium was characterized by X-ray diffraction and is shown in Figure 6. When adding the 2D phase, an additional diffraction peak appears at ~31° in 2θ that can be attributed to the (200) plane of the $Cs_2PbCl_2I_2$ phase. This main peak (and others) from the 2D phase are hardly seen when the 3D perovskite film is strongly textured. The occurrence of this peak has also been observed in a recent work for a $CsPbI_3/Cs_2PbCl_2I_2$ heterojunction obtained by depositing a layer of CsCl overlying $CsPbI_3$ and where the diffraction peak corresponding to the (200) plane of the 2D phase has a maximum intensity at 31.7° in 2θ.[37] In our study, the presence of texture explains the appearance of this single peak for the 2D phase and indicates not only a preferred orientation of this phase, but also that the (200) planes are under diffraction conditions and therefore parallel to the substrate. This observation would imply that the (00 l) planes of the 2D phase are oriented perpendicular to the substrate, as indicated by Li and coworkers in their work, without in their case evidencing for the presence of this particular diffraction peak.[38]

Based on these results, we can propose a schematic representation of the possible interface that can occur ideally in between the 3D structure of perovskite and the 2D material (see Figure 6). Although the interaction between the two phases can be at a macroscopic level or grain boundaries, it can also happen at the nanometer scale. If the growth process of the 3D material is preferentially favored along the $<$hh0$>$ and $<$00l$>$ directions for the black orthorhombic phase, it would necessarily mean that the corresponding family of planes are parallel to the substrate surface. For the 2D material, the $<$200$>$ direction is privileged and (h00) planes are therefore parallel to the substrate. The connections between the two phases is thus probably adjusted favorably at the outer plane interfaces of the 2D materials with an anchoring with the end of the 3D phases, facilitated by the octahedral tilts and the presence of the three types of anions.

The Pb–Pb distance is twice the value of d_{200} in the 2D phase, i.e. 5.98(1)Å, a value which is very close to the Pb–Pb distance of the $CsPbI_2Br$ phase estimated between 5.96 Å for

Research Article
doi.org/10.1002/ejic.202200490

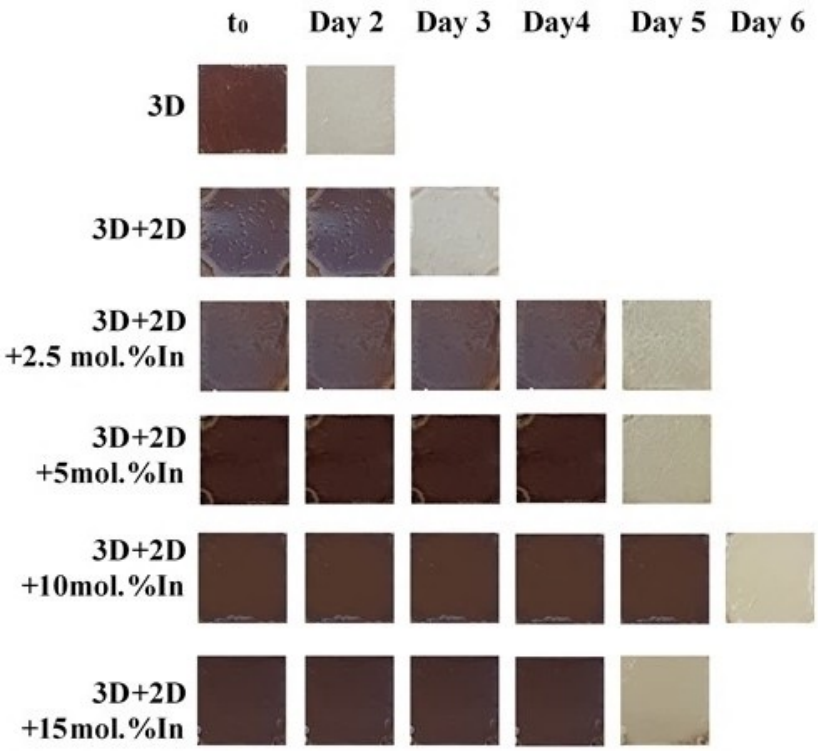

Figure 5. Images of perovskite thin films spin-coated on FTO/SnO_2 substrates (1×1 cm^2) and left in a vial for a few days.

the Pb–Br–Pb distance and 6.40 Å for the Pb–I–Pb distance, according to a previous study.[23] These values indicate a lattice mismatch of 0.3 and 7% respectively compared to the 2D phase. This same peak shifts slightly downward with the introduction of indium (though smaller in its trivalent state compared to lead) and disappears completely after adding 10% of indium. The peak located at 29.5° in 2θ corresponding to the black phase of $CsPbI_2Br$ shows a shoulder on the right with the introduction of the 2D phase which gradually disappears when the indium level increases. XRD data refinements by the Le Bail method were carried out on these patterns and made it possible to obtain the 3D structural lattice parameters values given for each composition in Figure 6. The presence of the 2D phase generates a contraction of the 3D phase unit cell because the parameters *a* and *b* decrease. This can be related to a phase anchoring at the interface between the 3D and 2D materials. A peak shift towards high angles in 2θ values corresponding to cell parameters decrease is consistent with a substitution on the lead site. As the indium rate increases, these *a* and *b* cell parameters come closer to finally be superimposed for 5 mol.% of indium. The introduction of indium would therefore make it possible to reduce the distortion of the orthorhombic structure of the 3D phase to tend towards a tetragonal structure. A significant improvement in the overall spatial symmetry with a closely packed atom arrangement due to the crystal structure transformation from orthorhombic to cubic was observed previously for an all-inorganic $InCl_3$:$CsPbI_2Br$ system.[28] The volume cell increases upon further doping, which signifies that a limit of solubility has been reached for ~5 mol. % of indium in the perovskite. We conclude that a combined indium substitution/insertion might occur at a higher doping level.

Fabrication, tests of [3D + 2D] solar cells and effects of indium

First, we used the standard conditions developed at XLIM for the preparation of each layer, with the deposition of the perovskite film in a glove box filled with N_2 (water and dioxygen concentrations < 1 ppm). The SnO_2 and Spiro-OMeTAD layers were respectively deposited before and after the perovskite layer in ambient air condition. The perovskite deposits on FTO/SnO_2 in a glove box have a different visual appearance from those obtained under nitrogen flow. A black color is noticed with inhomogeneities and a solvent front effect. After deposition of the Spiro-OMeTAD layer and the gold electrode, the characteristic color of the yellow phase reappears while the black phase seems to have completely disappeared. Therefore, it appears that the quality of the film is not sufficient by this method of preparation (under glove box) and that the deposition of the hole transporting layer destabilizes somehow the black phase of the perovskite, even when the deposition is carried out in an inert nitrogen atmosphere. This observation further confirms the importance of the optimization carried out previously using the nitrogen flow process.

Subsequently, all the deposits were carried out under simplified conditions of implementation under a nitrogen flow

Research Article
doi.org/10.1002/ejic.202200490

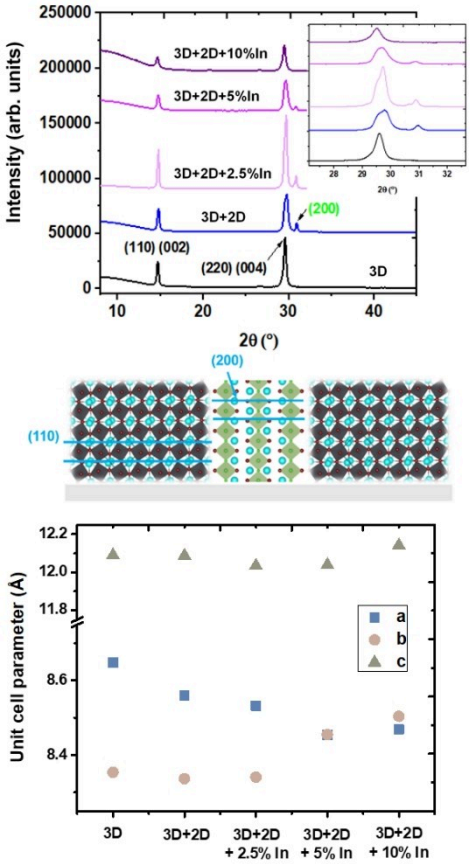

Figure 6. XRD patterns of inorganic halide $CsPbI_2Br$ perovskite-based thin films on FTO/SnO_2 substrates after our optimized three steps sequence. Preferred orientations are indexed (in green for the 2D phase). A schematic concept of the crystal assembling in between the 3D and 2D materials is shown. Unit cell parameters variations of the 3D $CsPbI_2Br$ phase.

and under a fume cupboard. The dark brown appearance characteristic of the black phase of $CsPbI_2Br$ perovskite is observed. However, a decrease in the surface area covered by the perovskite layer on the side of the gold electrode is also noticed, corresponding to a phase change towards the yellow phase. At this point, the first layer of FTO had been etched with acid and a zinc powder in order to be able to make the electrical contacts while avoiding short circuits. It thus appears that over the small width (1 to 2 mm) where the perovskite is deposited on the glass, it is not very stable and quickly turns yellow. This characteristic reflects the low stability of the perovskite layer when it is not constrained by the FTO/SnO_2 substrate. The deposit made in a glove box presents a lot of heterogeneities, holes and grains of sizes close to a micron. On the contrary, the film deposited under a flow of nitrogen has a smaller grain size, overall less than 100 nm, and is homogeneous. This difference in microstructure makes it possible to justify the destabilization of the black phase observed during the layering by Spiro-OMeTAD on the perovskite films treated in a glove box. Thus, although the literature generally recommends thermal deposition and treatment under these specific conditions, in our study, preparation of the film of the perovskite phase under nitrogen flow in ambient conditions visibly makes it possible to obtain films of better quality, which greatly facilitates the fabrication process.

For the $CsPbI_2Br$ phase, this technique made it possible to obtain working solar systems, with a "champion" device (with highest values of J_{sc}, V_{oc}, FF and η) with corresponding J(V) characteristics presented in Figure 7. The analyzes carried out in the dark (in black dotted lines), and under illumination towards positive voltages (in blue) and negative voltages (in green) are compared. A short-circuit current density (J_{sc}) of 15.6 mA/cm^2, an open circuit voltage (V_{oc}) of 0.91 V and a form factor (FF) of 0.63 are thus measured for a maximum photovoltaic efficiency

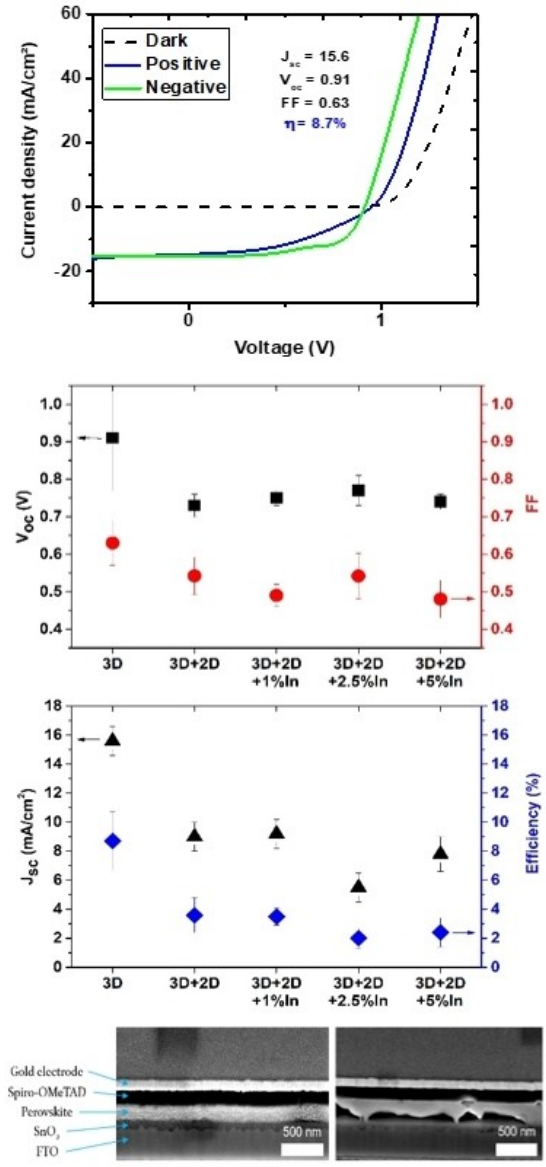

Figure 7. J(V) of our « champion » solar cell by using a $CsPbI_2Br$ perovskite layer. Short-circuit current density, open circuit voltage, form factor and photovoltaic conversion efficiency of different active layers based on the $CsPbI_2Br$ perovskite with the addition of the 2D $Cs_2PbCl_2I_2$ material (+7.5 mol. %) and indium. SEM side views images of (left) 3D $CsPbI_2Br$ and (right) [3D + 2D] mixture solar cells.

Research Article
doi.org/10.1002/ejic.202200490

conversion of 8.7%. A reasonable hysteresis phenomenon is observable, which results in a shift between the J(V) measurements made by sweeping towards positive and negative voltages. This phenomenon can be explained by an ionic migration in the material, which leads to an overestimation of the solar cell parameters for the scan performed in reverse mode (towards negative voltages).

From the deposits obtained under a nitrogen flow, complete photovoltaic devices could thus be produced. The chemical composition of the active layer was modulated to test the effects of the 2D phase and indium addition on the devices performances (see Figure 7). Despite the gain in film stability, the presence of the 2D phase and indium results in a decrease of the physical characteristics. SEM images produced in slices on the 3D phase cell alone and the [3D + 2D] mixtures show planar layers without discontinuities for the former, but a strongly reduced contact with the underlying SnO_2 layer is observed for the latter system. The stresses imposed by the addition of the 2D phase probably caused the perovskite layer to peel off and can explain for instance why the current collected in the case of the [3D + 2D] mixtures is lower than for the 3D phase alone. It therefore seems that optimizations still need to be carried out in order to perfect the contact between the perovskite layer and the electron transport layer. Using a mesoporous layer of TiO_2 rather than the SnO_2 layer, might for instance create a more mechanically coherent interface.

Texture and preferred orientation of thin films

The orientation of the crystalline planes with respect to the substrate places only certain families of planes in diffraction conditions and therefore makes it possible to observe only the inter-reticular distances of the planes positioned parallel to the substrate. The opposite of texture would be an isotropic polycrystalline material where all the diffraction planes are observable, related to a random distribution of crystallites in space. As a reminder, the XRD patterns showed in Figure 3 were obtained in the Bragg-Brentano θ–2θ configuration. In order to confirm the presence of texture, analyzes were carried out at the CEMES laboratory in Toulouse, France, on an X-ray diffractometer equipped with a (ψ, ϕ) cradle, a plane detector and an XYZ moving plate. The results obtained for these measurements are presented in Figure 8.

Diffraction images are read from small to large 2θ angles, from left to right. If we draw the horizontal line passing through the center of the detector image, we place ourselves in the condition where the tilt value corresponds to the angle ψ of the cradle (with ψ the angle between the vertical and the normal to the substrate). In Figure 8 the value is set to 0°, meaning that the positioning plate is strictly horizontal. On this diffraction image, a continuous ring is observed at 35.7° in 2θ (for a cobalt X-ray source), which corresponds to the main diffraction peak of the ITO substrate. Perovskite diffraction peaks appear in the form of circular arcs (or discontinuous rings). Two main diffraction peaks are observed for $\psi = 0°$, which are attributed to the (110) and (220) planes. The peak splits in the orthorhombic system are not discernible here, although the peak widths are significantly broad. In order to observe the (200) family of planes, it is necessary to tilt the specimen to $\psi = 20°$ (see Figure 8). A new diffraction arc thus appears at the top left of the diffraction image centered on $\psi = 45°$, which corresponds to the angle formed between the (110) and (200) planes in the crystal lattice of the gamma black form of the perovskite. This point is clearly visible in the (200) pole figure. The angular spreading in ψ of these diffraction arcs is 12°, which means that the corresponding planes are oriented parallel in a range of 12° (0 ± 6°) with respect to each other, reflecting the strong preferential orientation of our thin films. The corresponding pole figures, for a sample of $CsPbI_2Br$ deposited on FTO/SnO_2, are also shown in Figure 8. On one hand, it therefore appears that the texture is independent of

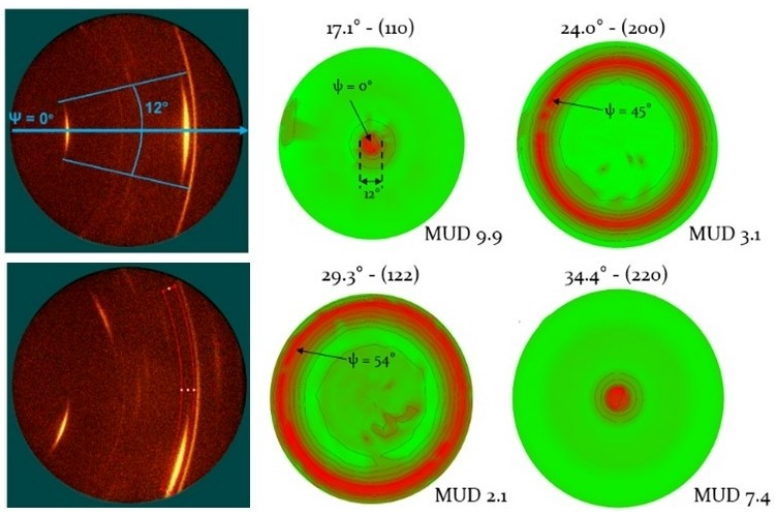

Figure 8. X-ray diffraction figures for a $CsPbI_2Br$ thin film on ITO substrate at (top left) $\psi \sim 0°$ and (bottom left) $\psi \sim 20°$. Measurements were performed at room temperature on freshly made thin films. (Right) Pole figures for a $CsPbI_2Br$ thin film based on integrated diffraction figures by using the red cursor.

Research Article
doi.org/10.1002/ejic.202200490

the substrate used since it can be observed both on deposits made on ITO and FTO/SnO_2. Deposits made on glass substrates (which are not presented here) also exhibit the same behavior in X-ray diffraction. The pole figures are read in polar coordinates, ψ evolves in radial position r, with r increasing from the center towards the outside of the pole figure between 0 and 60°, while ϕ (the sample rotation angle) varies with the angle around the circle θ between 0 and 360°. Thus, we can observe that the diffraction peaks attributed to the family of (hh0) planes are visible for ψ values ranging from $-6°$ to $+6°$, the diameter of the diffraction circle of the plane (110) being of about 12°, continuously for all ϕ values. The diffraction peaks attributed to the (200) planes are themselves visible between 39 and 51° in ψ (around 45°) while the (122) planes are centered on a value of $\psi = 54°$. This orientation was refined using DiffracTexture and Leptos software, and a fiber-like texture component was clearly reproducible in the $<110>$ direction parallel to the plane of the substrate. The MUD (Multiple of Uniform Density) parameter indicates the intensity of the texture observed by X-ray diffraction and is proportional to the crystal orientation. The crystal orientation distribution function (ODF) is defined by the volume fraction of crystals that have an orientation. It is normalized and this distribution is expressed in multiples of the uniform density. The value of this parameter is close to 7.4 for the reference and decreases to 5.8 when the 2D phase is added, which reflects a slight reduction in the crystal orientation probably induced by the formation of a heterojunction in the [3D + 2D] mixture. Adding 5% indium, which changes crystal growth and film microstructure to obtain spherically shaped grains, increases this factor to a value of 11.5. This observation confirms the contribution of indium to the organization of thin films at the structural level and illustrates a tendency for the increase in crystalline orientation brought about by this addition. During heat treatments in air, the solvent evaporates not homogeneously and results in the formation of large isolated grains with poor contact between them. The planes are furthermore randomly distributed in all directions of space since the diffraction planes of different families can be observed by X-ray diffraction with a punctual detector. When using nitrogen flow, reducing the thickness of the boundary layer allows the solvent to evaporate homogeneously. The film formed by this process has small grains (of the order of 100 nm), which are however compactly crystallized and cover the entire substrate. The fiber-like texture also indicates that the grains are all oriented with continuity with almost perfect alignment of the diffraction planes of the same family in a single direction of space. Scratching the sample and complementary high resolution transmission electron microscopy (HR-TEM) analyzes on films have been considered in an attempt to verify these phenomena, but these are difficult to perform given the instability of the films under intense electron beam. Texture induced by the crystallization process after spin-coating are important for the stability of thin films. Although these parameters are increasingly described in the literature, it would be interesting to systematically integrate them in stability studies, given their influence on ionic migration and the interfaces between thin layers. The importance of the gas flow used during the crystallization step of the perovskite layer was evidenced and it is possible to manufacture thin films under less drastic conditions than in a glove box, allowing to consider more serenely this technology upscaling.

Therefore, the novel 2D/3D approach has proven ability in stabilizing perovskite solar cells, in both fully inorganic or hybrid organic/inorganic systems, but simultaneous improvements in efficiency and stability will bring further this technology. Self-assembled monolayers (SAMs) usually based on carbazole bodies with phosphonic acid can be used for perovskite layers and interfaces with electrodes anchoring and stabilization, device alignment and passivation defects. For this purpose also, additives, essentially introduced during perovskite film formation, such as Lewis acids (PbI_2…) or bases (O-, S-, or N-donor types), ammonium salts, ionic liquids and other low-dimensional perovskites can be efficient alternatives. To avoid moisture and oxygen degradation, interfacial engineering to improve charge transport is really useful for perovskite solar cell evolution by using metal oxides, ternary or quaternary cations, and organic carbon-based layers.[41] By combining these solutions, some hybrid-based solar cells have already achieved PCE above 20% with lifetimes of 10 000 h in storage. Finally, the encapsulation and recyclability of the devices will also strongly contribute to an extended industrial production.

Conclusion

Thin films of crystalline $CsPbI_2Br$-based materials were made by a simple process, in a conventional laboratory environment. A nitrogen flow deposition process was used to minimize surface defects and preserve perovskite black phase. Indium was then selected, primarily for steric compliance reasons, to substitute for lead in perovskite. The microstructure of the [3D + 2D] mixture has a homogeneous grain size and optimum compactness for 5 mol. % indium with respect to 3D phase. The orthorhombic distortion of the structure is lowered (it tends towards a tetragonal symmetry) and the black phase of the perovskite remains present the longest (5 days in normal atmosphere) for an indium rate close to 10%. A maximum conversion efficiency close to 9% was measured for the pure $CsPbI_2Br$ material. While the black phase is stabilized upon addition of the 2D phase and indium doping, the solar cell efficiency is decreased by about 3 order of magnitudes. Finally, a textural study showed that (110) crystalline planes are predominantly oriented parallel to the substrate. The most stable films, composed of a [3D + 2D] mixture with 5 mol. % In, show the strongest preferential orientation. These texturing effects are correlated with the presence of crystalline distortions reduction that stabilize the black phase.

Experimental section

Solutions of 3D $CsPbI_2Br$ (1.5 M) were produced by mixing 1.5 mmol of CsI (99.9% from Sigma-Aldrich) with 0.75 mmol of PbI_2 (99% from Sigma-Aldrich) and 0.75 mmol of $PbBr_2$ (98% from Alfa-Aesar) for 2 hours with 1 mL of dimethyl sulfoxide (DMSO) at room

temperature. The type of solvent used strongly influences crystallization, where DMSO is much less volatile and toxic than dimethyl formamide (DMF). For the mixture of the 3D and 2D phases, 0.1125 mmol of the 2D material was added to 1 mL of 3D solutions before mixing for a couple of hours and filtering with a 0.2 μm polytetrafluoroethylene PTFE filter.

An aqueous colloidal solution of SnO_2 nanoparticles was prepared by using a commercial suspension from Alfa Aesar (15 wt.% in water) mixed with 1 vol.% of isopropanol. The SnO_2 nanoparticles layer was deposited by spin-coating in a single step and treated at 150 °C for 30 minutes in air.

73.2 mg of 2,2′,7,7′-tetrakis(*N*,*N*-di-p-methoxyphenyl-amine)-9,9′-spirobifluorene or Spiro-OMeTAD (99% from Sigma-Aldrich) were dissolved in 1 mL of chlorobenzene while 106 mg of lithium bis(trifluoromethane)sulfonimide Li-TFSI was dissolved in 200 μL of acetonitrile. 17.5 μL of this solution and 28.8 μL of 4-ter-butylpyridine were mixed together in the Spiro-OMeTAD solution, which was then filtered.

Commercial 1 mm thick glass samples (3×3 cm^2) were purchased from Solems with 80 nm (Indium Tin Oxide) ITO or (Fluoride Tin Oxide) FTO pre-deposited layers, respectively of an electrical resistance of 30 or 80 Ohms. Samples were cut manually to about 1×1 cm^2 before washing successively with acetone and ethanol for 15 minutes under sonication. Each substrate is then treated under UV-ozone for 25 minutes.

The deposition conditions (speed and acceleration rate in the case of spin-coating) were adjusted thoroughly based on the solution/substrate system used, all in order to obtain the desired thickness and thin film microstructure, generally comprised in between 300 and 800 nm in thickness, depending on the shape and compactness of grains formed.

The architecture used for the devices produced in this work is based on the stacking of layers usually described in the literature to ensure optimal load transfer.[39] This work was carried out at the XLIM laboratory in Limoges, France, initially optimized for multication compositions of $(FA,Cs)Pb(I,Br)_3$ where FA^+ stands for formamidinium cations.[40] The final stack is as follows: a commercial glass substrate covered with a layer of approximately 300 nm FTO (transparent semiconductor), on which are successively deposited by spin-coating, using a SPS spin 150 apparatus, the layers of SnO_2 nanoparticles (acting as an electron transport layer with a thickness of 50 nm), the active layer of perovskite (~300 nm) and Spiro-OMeTAD (hole transport layer, 200 nm thick). The cell is finally completed by a thermally evaporated gold film under high vacuum at 10^{-6} mbar to form the counter-electrode (~100 nm).

For low magnification Scanning Electron Microscopy (SEM) images, a VEGA3-Tescan apparatus was used, equipped with a tungsten source and Energy Dispersive Spectroscopy with X-ray emissions (EDX) Brüker detector with 30 kV tension and 10 pA beam intensity. For high magnification images (>100 000), FEI HELIOS 600i Field Emission Gun/Focused Ion Beam (FEG/FIB) microscope was used with 5 kV tension.

X-Ray Diffraction (XRD) patterns recorded at room temperature in the Bragg-Brentano geometry were obtained at CIRIMAT laboratory on a Brüker AXS D8-Advance apparatus equipped with a copper cathode (K-alpha1 = 1.5406 Å and K-alpha2 = 1.5443 Å) and a LynxEye detector. Data were collected from 8 to 100° in 2θ angles, within 15 minutes.

XRD images were measured at room temperature at CEMES laboratory using a Brüker D8-Discover apparatus and a cobalt micro-source cathode (K-alpha1 = 1.7897 Å) with a spot size of 1 mm. The sample is mounted on a cradle equipped with two rotation axes and a three-axis positioning plate (xyz stage). A Vantec 500 2D detector with 30° angular opening at a distance of 20 cm from the sample has been used.

Current-Voltage (I–V) characteristics measurements have been realized in ambient conditions without encapsulation using an interfaced Keithley 2400 source-measure unit and a NEWPORT 1600 W solar simulator equipped with a AM1.5G filter. The calibration of the solar simulator was made using a certified reference single crystalline silicon cell from NEWPORT, taking into account the typical mismatch factor associated with $(FA,Cs)Pb(I,Br)_3$ reference perovskite. The irradiance was set to 100 mW/cm^2 in these conditions for the reference device.

Acknowledgments

We would like to thank Benjamin Duployer and Yann Borjon-Piron for their assistance in X-ray diffraction and Scanning Electron Microscopy analysis, respectively. This work was supported by institutional grants from the National Research Agency under the Investments for the future program with the reference ANR-10-LABX-0074-01 Sigma-LIM. Device processing was performed within the PLATINOM technology platform of XLIM Research institute (common facility of the University of Limoges). Part of the experiments were granted through a "Nouvelle Aquitaine" regional project. The authors would like to acknowledge also the HPERO Research network (CNRS MITI) for financial support.

Conflict of Interest

The authors declare no conflict of interest.

Data Availability Statement

The data that support the findings of this study are available from the corresponding author upon reasonable request.

Keywords: Halide perovskites · Indium-Doping · Solar Cells · Thin Films · Two-Dimensional (2D) Structures

[1] N. K. Kumawat, X.-K. Liu, D. Kabra, F. Gao, *Nanoscale* **2019**, *11*, 2109.
[2] S. D. Stranks, P. K. Nayak, W. Zhang, T. Stergiopoulos, H. J. Snaith, *Angew. Chem. Int. Ed.* **2015**, *54*, 3240.
[3] T. Yang, F. Li, R. Zheng, *Mater. Adv.* **2021**, *2*, 6744.
[4] T. Ma, S. Wang, Y. Zhang, K. Zhang, L. Yi, *J. Mater. Sci.* **2020**, *55*, 464.
[5] B. Li, Y. Zhang, L. Fu, T. Yu, S. Zhou, L. Zhang, L. Yin, *Nat. Commun.* **2018**, *9*, 1076.
[6] G. E. Eperon, G. M. Paterno, R. S. Hawke, A. Zampetti, A. A. Haghighirad, F. Cacialli, H. J. Snaith, *J. Mater. Chem. A* **2015**, *3*, 19688.
[7] W. Chen, D. Li, X. Chen, H. Chen, S. Liu, H. Yang, X. Li, Y. Shen, X. Ou, Y. Yang, L. Jiang, Y. Li, Y. Li, *Adv. Funct. Mater.* **2022**, *32*, 2109321.
[8] H. Chen, Q. Cheng, H. Liu, S. Cheng, S. Wang, W. Chen, Y. Shen, X. Li, H. Yang, H. Yang, J. Xi, Z. chen, X. Lu, H. Lin, Y. Li, Y. Li, *Sci. Bull.* **2022**, *67*, 1243.
[9] T. Ozturk, E. Akman, A. E. Shalan, S. Akin, *Nano Energy* **2021**, *87*, 106157.
[10] E. Breniaux, P. Dufour, S. Guillemet-Fritsch, C. Tenailleau, *Eur. J. Inorg. Chem.* **2021**, *30*, 3059.
[11] J. Li, Y. He, C. C. Stoumpos, G. Niu, G. G. Trimarchi, H. Guo, G. Dong, D. Wang, L. Wang, M. G. Kanatzidis, *J. Am. Chem. Soc.* **2018**, *140*, 11085.

[12] L.-Y. Pan, Y.-F. Ding, Z.-L. Yu, Q. Wan, B. Liu, M.-Q. Cai, *J. Power Sources* **2020**, *451*, 227732.
[13] E. Breniaux, E. J. Marin-Bernardez, E. Gallet, P. Dufour, C. Tenailleau, *Mater. Chem. Phys.* **2020**, *247*, 122870.
[14] S. Wang, C. Zhang, Y. Feng, Y. Shao, Y. Yan, Q. Dong, J. Liu, B. Hu, S. Jin, Y. Shi, *J. Mater. Chem. A* **2018**, *6*, 8860.
[15] T. Mori, H. Okada, V. O. Eze, Y. Seike, *J. Photopolym. Sci. Technol.* **2020**, 33, 399.
[16] S. S. Mali, J. V. Patil, J. A. Steele, S. R. Rondiya, N. Y. Dzade, C. K. Hong, *ACS Energy Lett.* **2021**, *6*, 778.
[17] C. Zhou, T. Zhang, C. Zhang, X. Liu, J. Wang, J. Lin, X. Chen, *Adv. Sci.* **2022**, *9*, 2103491.
[18] S. Wang, C. Zhang, Y. Feng, Y. Shao, Y. Yan, Q. Dong, J. Liu, B. Hu, S. Jine, Y. Shi, *Nanotechnol. Energy* **2014**, *10*, 10.
[19] A. Babayigit, J. D'Haen, H.-G. Boyen, B. Conings, *Joule* **2018**, *2*, 1205.
[20] S. Chen, X. Xiao, B. Chen, L. L. Kelly, J. J. Zhao, Y. Lin, M. F. Toney, J. Huang, *Sci. Adv.* **2021**, *7*, 2412.
[21] L.-L. Gao, K.-J. Zhang, N. Chen, G.-J. Yang, *J. Mater. Chem. A* **2017**, *5*, 18120.
[22] X. Zhao, T. Liu, Q. C. Burlingame, T. Liu, R. Holley, G. Cheng, N. Yao, F. Gao, Y–L. Loo *Science* **2022**, *377*, 307.
[23] W. Chen, H. Chen, G. Xu, R. Xue, S. Wang, Y. Li, Y. Li, *Joule* **2019**, *3*, 191.
[24] W. S. Subhani, K. Wang, M. Du, S. F. Liu, *Nano Energy* **2019**, *61*, 165.
[25] J. Liang, X. Han, J–H. Yang, B. Zhang, Q. Fang, J. Zhang, Q. Ai, M. M. Ogle, T. Terlier, A. A. Martí, J. Lou, *Adv. Mater.* **2019**, *31*, e1903448.
[26] U. Khan, Y. Zhinong, A. A. Khan, A. Zulfiqar, N. Ullah, *Nanoscale Res. Lett.* **2019**, **14**, 116.
[27] J. V. Patil, S. S. Mali, C. K. Hong, *J. Energy Chem.* **2021**, *62*, 451.
[28] C. Liu, W. Li, H. Li, H. Wang, C. Zhang, Y. Yang, X. Gao, Q. Xue, H–L. Yip, J. Fan, R. E. I. Schropp, Y. Mai, *Adv. Energy Mater.* **2019**, *9*, 1803572.
[29] X. Li, K. Wang, F. Lgbari, C. Dong, W. Yang, C. Ma, H. Ma, Z.-K. Wang, L–S. Liao, *Nano Res.* **2020**, *13*, 2203.
[30] J. A. J. Pardoe, A. J. Downs, *Chem. Rev.* **2007**, 107, 1, 2.
[31] Y. Hu, F. Bai, X. Liu, Q. Ji, X. Miao, T. Qiu, S. Zhang, *Energy Lett.* **2017**, *2*, 2219.
[32] T. Zhang, M. I. Dar, G. Li, F. Xu, N. Guo, M. Grätzel, Y. Zhao, *Sci. Adv.* **2017**, *3*, 1700841.
[33] L. McGovern, I. Koschany, G. Grimaldi, L. A. Muscarella, B. Ehrler, *J. Phys. Chem. Lett.* **2021**, *12*, 2423.
[34] Q. An, F. Paulus, D. Becker-Koch, C. Cho, Q. Sun, A. Weu, S. Bitton, N. Tessler, Y. Vaynzof, *Matter* **2021**, *4*, 1683.
[35] D. Kim, K. Higgins, M. Ahmadi, *Matter* **2021**, *4*, 1442.
[36] J.-S. Park, J. Calbo, Y.-K. Jung, L. D. Whalley, A. Walsh, *Energy Lett.* **2019**, *4*, 1321.
[37] H. Wang, H. Liu, Z. Dong, T. Song, W. Li, L. Zhu, Y. Bai, H. Chen, *Nano Energy* **2021**, *89*, 106411.
[38] Z. Li, X. Liu, J. Xu, S. Yang, H. Zhao, H. Huang, S. F. Liu, J. Yao, *J. Phys. Chem. Lett.* **2020**, *11*, 4138.
[39] S. S. Shin, E. J. Yeom, W. S. Yang, S. Hur, M. G. Kim, J. Seo, J. H. Noh, S. I. Seok, *Science* **2017**, *356*, 167.
[40] S. Karthick, H. Hawashin, N. Parou, S. Vedraine, S. Velumani, J. Bouclé, *Sol. Energy* **2021**, *218*, 226.
[41] A. Urbina, *J. Phys. E* **2020**, *2*, 022001.

Manuscript received: August 1, 2022
Revised manuscript received: September 21, 2022
Accepted manuscript online: September 21, 2022